DFT Design of Inhibitors of the LpxC Enzyme

Carolyn Dishuck

Department of Biology

Rhodes College

Memphis, TN

2017

Submitted in partial fulfillment of the requirements for the Bachelor of Science Degree with Honors in Biology

This Honors paper by Carolyn Frances Dishuck has been read and approved for Honors in the Department of Biology

Dr. Mauricio Cafiero

Project Advisor

_____

Dr. Larryn W. Peterson

Second Reader

_____

Dr. Bayly Wheeler

Extra-Departmental Reader

_____

Dr. Carolyn Jaslow

Department Chair

_____

\

Acknowledgements

National Science Foundation Grant CHE-1229354

Rhodes Fellowships Program

Rhodes College, Department of Chemistry

Rhodes College, Department of Biology

Dr. Mauricio Cafiero

Dr. Larryn Peterson

Dr. Carolyn Jaslow

Contents

Signature Page	ii
Acknowledgements	iii
Contents	iv
List of Figures and Tables	v
Abstract	1
Introduction	2
Computational Methods	4
Results and Discussion	6
Conclusion	27
Bibliography	29

List of Figures

Figure 1: Lipid A is a crucial component of the LPS of the outer membrane of Gram-negative bacteria, without which the bacteria cannot survive. 2

Figure 2: Biosynthesis of lipid A. LpxC removes the acetyl group from the nitrogen on the sugar ring. 3

Figure 3: General design of proposed inhibitors. The hydroxamic acid serves as the zinc binding region and will be constant among the proposed inhibitors. 4

Figure 4: Proposed inhibitors. The linker, nucleoside, and hydrophobic moiety are systematically varied. 6

Figure 5: Possible modes of binding to Zn^{2+}. 7

Figure 6: Solvent optimized structures. The purple atom is Zn^{2+}. 8

Figure 7: Water cluster structures used in desolvation studies. 12

Figure 8: CR-2.2 optimized in the active site of LpxC. The purple atom is Zn^{2+}. 14

Figure 9: Proposed inhibitors. The linker, nucleoside, and hydrophobic moiety are systematically varied. 15

Figure 10: CR-6 optimized complex. The purple atom is Zn^{2+}. 16

Figure 11: Proposed ligands for Eckenhoff's Zn^{2+} binding model. 20

Figure 12: Crystal structure of model active site and eck. 20

Figure 13: Molecular orbitals for the hydroxamic acid eckenhoff model excited states. 23

Figure 14: Molecular orbitals for the carboxylic acid eckenhoff model excited states. 24

List of Tables

Table 1: Interaction energies of the vacuum model. Results are in kcal/mol. 7

Table 2: Interaction energies of the solvent model. Results are in kcal/mol. 9

Table 3: Simplified Zn^{2+} binding model version one. Interaction energies are in kcal/mol. 10

Table 4: Simplified Zn^{2+} binding model version two. Interaction energies are in kcal/mol. 10

Table 5: Desolvation energies – version one. Results are in kcal/mol. 11

Table 6: Desolvation energies – version two. Results are in kcal/mol. 11

Table 7: Electronic binding energies. Results are in kcal/mol. 11

Table 8: Interaction energies in kcal/mol for CR-2.2 and CR-6. 18

Table 9: Eckenhoff model bond length comparisons and electronic excitation energies. Bond lengths are in angstroms. 21

Table 10: Carboxyl Eckenhoff model bond length comparisons and electronic excitation energies. Bond lengths are in angstroms. 22

Table 11: Log P for the protonated forms of the molecules. 25

Table 12: Log P for the deprotonated forms of the molecules. 26

Table 13: Log D values. 27

Abstract

In recent years bacterial infections have become more resistant to treatments, posing a challenge for both researchers and health professionals. It has become imperative that novel, effective therapies against these resistant bacterial infections be discovered. Gram-negative bacteria present an additional challenge due to the presence of a selectively permeable outer membrane. Among the components of the outer membrane is Lipid A, which is responsible for the growth and pathogenicity of Gram-negative bacteria. The enzyme LpxC, a zinc-dependent deacetylase, is responsible for catalyzing the first committed step in the biosynthetic pathway of Lipid A. The inhibition of LpxC would therefore, prevent the production of Lipid A, and hence result in a corrupted outer membrane. Starting from an LpxC crystal structure with a natural substrate bound in the active site, we have designed and optimized the position of several novel ligands in the active site. The structure for these ligand-protein complexes were optimized using M06l and the 6-31G basis set both *in vacuo* and in solution phase. Interaction energies for the ligand and protein complex were calculated using M06l with the 6-311+G* basis set. Desolvation and simplified zinc binding studies have also been performed to confirm that our model chemistry describes the zinc binding in the protein appropriately. Additionally, Log P and Log D have been computationally calculated to determine whether the molecules may be biologically active. Initial work shows several promising candidates for the inhibition of LpxC.

1. Introduction

In recent years, bacterial resistance has become a challenge for both researchers and health professionals in developing antibacterial treatments and treating bacterial infections, respectively. Due to their selectively permeable outer membrane, which confers increased resistance to antibacterial treatment, Gram-negative bacteria, when compared to Gram-positive bacteria, pose an additional threat. Not only does the outer membrane increase bacterial resistance, its components can also lead to serious health risks. Lipid A, a crucial component of the lipopolysaccharide (LPS) of the outer membrane and a potent toxin, can lead to septicemia when released from dying bacterial cells (Figure 1).[1,2] Septicemia was the 10th leading cause of death in the United States in 2010.[3]

Studies have illustrated that lipid A is crucial for the growth and virulence of Gram-negative bacteria and that reduced levels of the lipid increase the sensitivity of Gram-negative bacteria to antibiotics.[4,5] For these reasons, the inhibition of the biosynthesis of lipid A is an attractive approach for developing novel antibacterial treatments.

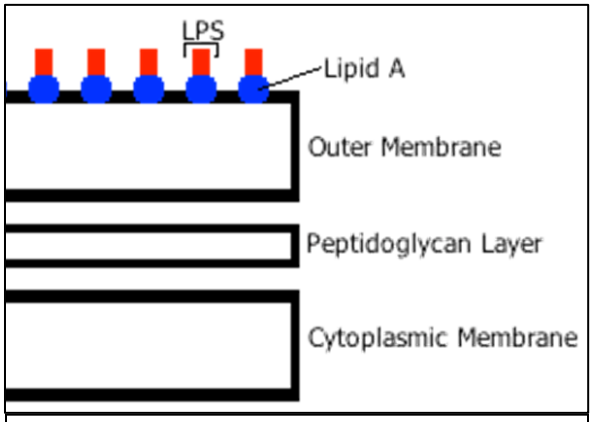

Figure 1: Lipid A is a crucial component of the LPS of the outer membrane of Gram-negative bacteria, without which the bacteria cannot survive.[1]

A zinc dependent deacetylase, uridinyldiphospho-3-O-(R-3-hydroxymyristoyl)-N-acetylglucosamine deacetylase (LpxC), catalyzes the first committed step in the biosynthesis of lipid A (Figure 2).[4,5] The acetyl group of UDP-3-O-(R-3-hydroxymyristoyl)-N-acetylglucosamine is cleaved by LpxC. This results in a free amino group, which LpxD conjugates to an R-3-hydroxymyristoyl chain. Conveniently, no other known mammalian

enzymes are homologous in sequence to LpxC. Therefore, targeting this enzyme confers little risk of toxicity.[6-8]

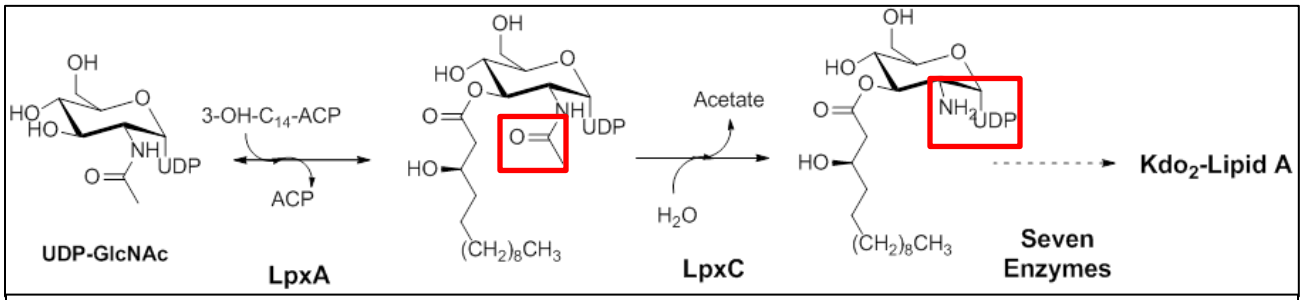

Figure 2: Biosynthesis of lipid A. LpxC removes the acetyl group from the nitrogen on the sugar ring.[15]

LpxC has been crystallized with its natural substrate, uridine diphosphate (UDP), in the active site (PDB ID:2IER). Additionally, several inhibitors of LpxC have been discovered.[2, 5, 8-12]

In the paper "Antibacterial agents that inhibit lipid A biosynthesis" by Onishi et al, the researchers describe analogs that inhibit LpxC. They identified L-161,240 as one of the most effective inhibitors.[5] Additionally, in studies with mice, their compounds were shown to cure *E.coli* infection.[5]

Another study that characterizes inhibitors of LpxC is "Antibacterial activities and characterization of novel inhibitors of LpxC" by Clements et al. This study identifies a series of sulfonamide derivatives that inhibit LpxC. Notably, these ligands included a hydroxamic acid portion.[10]

Analyzing the interactions of these inhibitors and of UDP in the active sight of LpxC gives us insight into the most important structural components involved in ligand binding.[13,14] These include a Zn^{2+} binding group, a hydrophobic moiety, and a nucleoside (Figure 3).

This knowledge of LpxC and its active site has been used in our design of several novel ligands, which have been analyzed computationally.

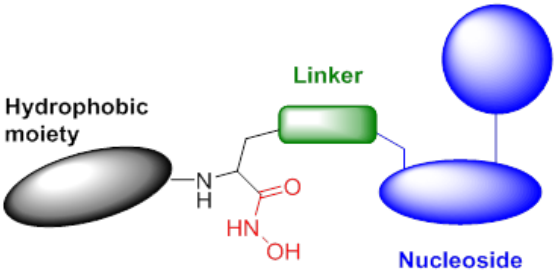

Figure 3: General design of proposed inhibitors. The hydroxamic acid serves as the zinc binding region and will be constant among the proposed inhibitors.

2. Computational Methods

Starting from the LpxC crystal structure with the natural substrate bound in the active site (PDB ID:2IER), proposed analogues were docked in the active site. The active site was determined by selecting amino acids most proximal to the natural substrate. Most optimizations were completed using M06l/6-31G. M06l was used since it is better for active sites with metals.[22] A relaxed active site where the heavy atoms on the amino acid side chains and all protons were allowed to adjust their positions was used. Optimizations with implicit solvation were done via the PCM model using default parameters.[23] The solvent in these cases was water. Interaction energies were also calculated from the solvent optimized structures. In all cases, counterpoise corrected interaction energies were calculated for the ligand/amino acid pairs and ligand/ Zn^{2+} using M06l/6-311+G*. Calculations were performed using Gaussian09.[16]

In our desolvation studies, desolvation energies for the ligands and Zn^{2+} were calculated using M06l/cc-pvdz using six water molecules for the Zn^{2+}, nine water molecules for molecules CR-2 through CR-5, and ten water molecules for CR-1. The six water molecule starting structure was

taken from Wang et al.[17] The nine water molecule starting structure, as well as the ten water molecule starting structure was taken from Perez et al.[18]

Time dependent DFT was used to calculate the electronic excitation energies for the Zn^{2+} binding models.

Computational measures of partition coefficients (LogP) were determined for both the first and second generation ligands. LogP was determined for ligands with all ionizable substituents fully protonated, while LogD considers the ligand at physiological pH. For determination of LogP, ligands were optimized twice with B3LYP/6-311+G* using n-octanol and water via PCM for the optimizations, separately. The harmonic vibrational frequencies of the ligands were determined in the optimization, producing the total free energy of the molecule (**Δ**Gtotal).

A relative value for pKa was determined computationally using B3LYP/3-21G*, applying implicit solvation via the PCM model. The pKa of both the acidic (protonated) form and basic (neutral) form of the ligand were determined using the described method. Once pKa values and partition coefficient values were obtained, the relative values of LogD were determined for all ligands, which could be ionized at physiological pH.[20,21]

3. Results and Discussion

Optimizations with Truncated Active Site – Vacuum Model

Five first generation molecules were proposed for study. These are CR-1 through CR-5 (Figure 4). These molecules do not include a hydrophobic moiety, as this would increase the amount of computational resources necessary to complete optimization of the molecules. The larger the molecule, the more computationally expensive optimization becomes.

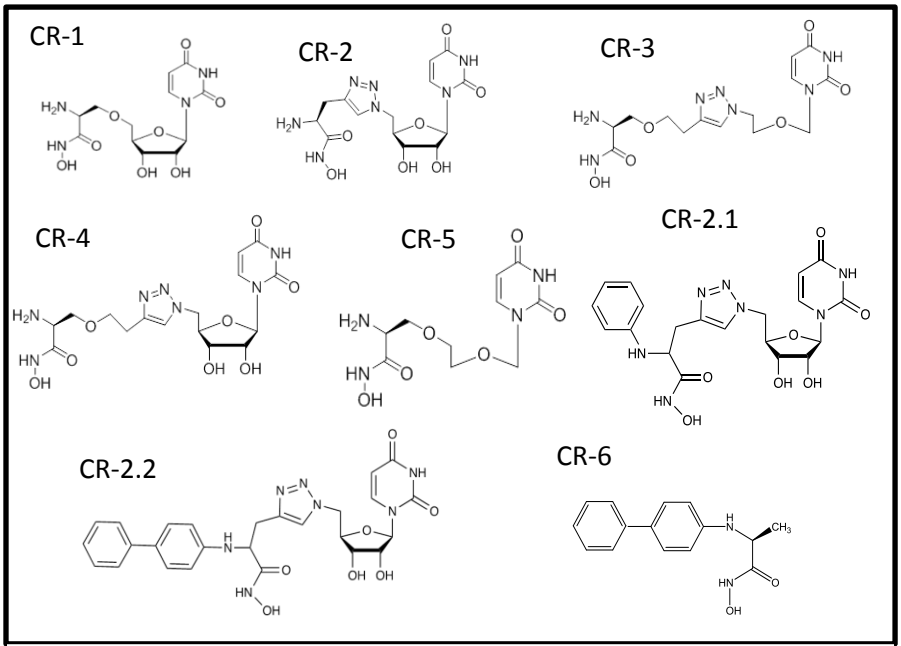

Figure 4: Proposed inhibitors. The linker, nucleoside, and hydrophobic moiety are systematically varied.

The five first generation molecules were optimized using a truncated active site which includes His265, Gly264, His58, Phe192, Phe194, Glu197, and Lys239. A vacuum model was first completed followed by a solvent model. For the solvent model we used implicit solvation with water via the PCM model using default parameters. Interaction energies were calculated for the ligand and Zn^{2+} and the ligand and amino acid residues in both conditions.

Since the Zn^{2+} in the active site has a positive charge it can bind with any portion of the substrate that is partially negative. Each of the atoms with which Zn^{2+} may interact

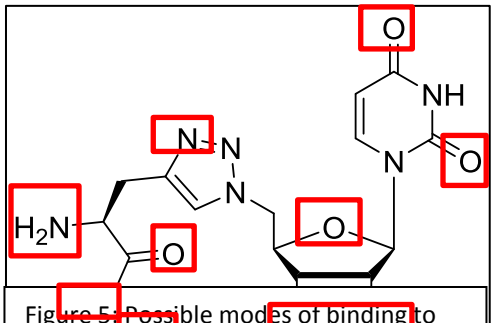

Figure 5: Possible modes of binding to Zn^{2+}.

are boxed in red in Figure 5. The natural substrate of LpxC binds Zn^{2+} using the oxygens of the hydroxamic acid, producing a very strong attractive interaction.

The results of the vacuum model are shown in Table 1. This data was collected by a previous member of our research team. Negative numbers indicate attractive forces between the amino acids and the ligand; positive numbers show repulsive forces. It was concluded that CR-5 exhibits the strongest interaction due to the rotational freedom around its bonds. That is, it is able to adjust its position in the active site to interact most favorably.

Table 1: Interaction energies of the vacuum model. Results are in kcal/mol.

		CR-1	CR-2	CR-3	CR-4	CR-5
Ligand and Zn		-282	-496	-296	-293	-438
Ligand and His		0.730	-117	-2.94	-194	1.56
Ligand and Phe		-1.70	7.20	-9.32	-9.24	1.74
Ligand and Glu		-36.96	x	-11.33	2.94	-19.84
Ligand and Lys		-38.18	x	-27.81	-31.77	-109.23
Total		-549.16	-613.94	-544.76	-529.37	-767.11

Optimizations with Truncated Active Site - Solvent Model

Figure 6 illustrates the optimized complexes of the solvent model. Molecules CR-2, CR-3, CR-4, and CR-5 all bound Zn^{2+} through the hydroxamic acid oxygens, as intended. CR-2, CR-3, and CR-4 also bound Zn^{2+} with their triazole rings. CR-5 bound Zn^{2+} with its NH_2. CR-1 bound Zn^{2+} with the oxygen on the uracil, an oxygen on the sugar, and NH_2.

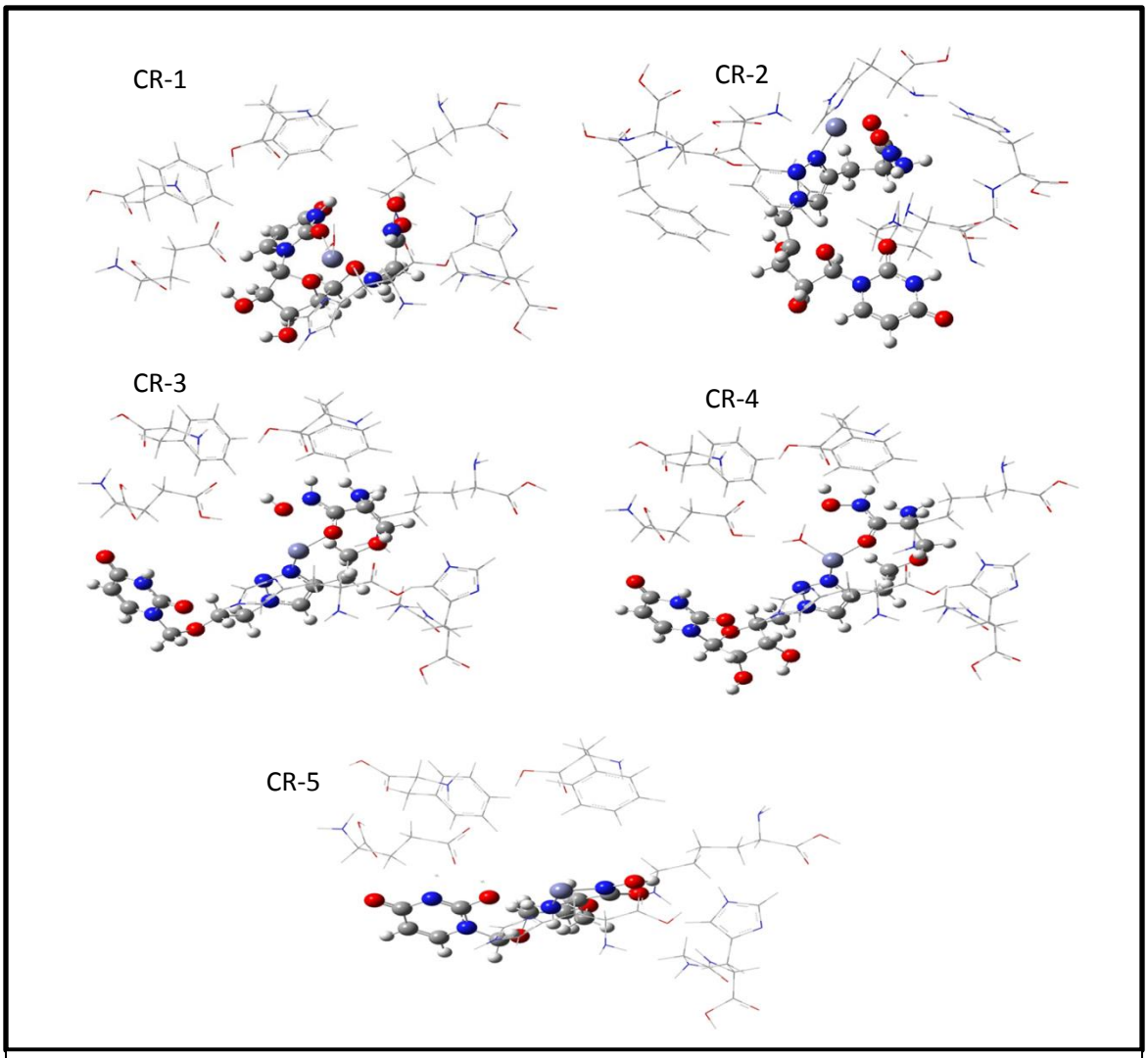

Figure 6: Solvent optimized structures. The purple atom is Zn^{2+}.

The results of the counterpoise corrected interaction energies of the solvent model are summarized in Table 2. It was concluded that CR-2 exhibits the strongest interaction because of the hydroxamic acid oxygen interacting with the backbone NH_2 of the histidine residue. This is a strong hydrogen bonding interaction. The solvent model can be considered a more realistic model, as it is more representative of the conditions in vivo.

Table 2: Interaction energies of the solvent model. Results are in kcal/mol.

		CR-1	CR-2	CR-3	CR-4	CR-5
Ligand and Zn		-287.34	-491.50	X	X	-448.49
Ligand and His		0.16	-110.51	X	-1.57	0.81
Ligand and Phe		-0.16	0.74	X	-9.84	0.74
Ligand and Glu		-10.34	-9.42	X	2.25	-10.34
Ligand and Lys		-34.64	-92.10	X	-28.24	-113.22
Total		-354.65	-710.50	X	X	-584.55

Interaction Energies in a Simplified Model

Our next step was to study a simplified Zn^{2+} binding model in order to provide our experimental collaborators with data with which to compare their Zn^{2+} binding assays. The results are summarized in Table 3 and Table 4. The difference between versions one and two is the orientation of the ligand with respect to Zn^{2+}. Version one was taken from the optimized solvent model structures. All molecules were removed except for our ligand, the Zn^{2+} ion, and the histidine of the active site, which was necessary to hold the Zn^{2+} ion in place. Version two was taken from version one, with the hydroxamic acid of the ligand being rotated around its bond in order to possibly induce a different mode of binding. In version one, CR-4 binds most favorably to zinc, while in version two CR-3 binds most favorably to zinc.

Table 3: Simplified Zn^{2+} binding model version one. Interaction energies are in kcal/mol.

	CR-1	CR-2	CR-3	CR-4	CR-5
Ligand and Zn^{2+}	-69.16	-79.20	-102.35	-104.67	-38.88

Table 4: Simplified Zn^{2+} binding model version two. Interaction energies are in kcal/mol.

	CR-1	CR-2	CR-3	CR-4	CR-5
Ligand and Zn^{2+}	-30.98	-35.53	-103.49	-83.30	-96.62

Desolvation Energies

Following the Zn^{2+} binding model, we set out to determine the electronic binding energies of our ligands. The electronic binding energies of the ligands to the active site are assumed to be a sum of three contributions, that of the electronic interaction energy between the ligand and the active site residues, the desolvation energy of the ligand and the active site, and the rearrangement energy of the entire molecular system upon ligand binding. Since we aim only to identify relative electronic binding energies, we can assume that the only significant contributor to desolvation energy will be the desolvation of the ligand; the ligands will displace a constant number of water molecules upon binding to the active site. The rearrangement energies are also taken to be constant across all ligands. Therefore, for the relative electronic binding energy, we can sum the electronic interaction energies and the desolvation energy of the ligand.[19] Following this logic, we have calculated the total binding energies of our ligands CR-1 through CR-5. The desolvation energies of versions one and versions two are shown in Table 5 and Table 6, respectively. The total electronic binding energies are shown in Table 7. These values are the sum of the total interaction energies in solvent and the average of the desolvation energies from version one and version two. The water cluster structures used in this study can be seen in Figure 7.

Table 5: Desolvation energies – version one. Results are in kcal/mol.

Zn^{2+}	CR-1	CR-2	CR-3	CR-4	CR-5*
381.62	31.91	65.97	23.02	36.47	27.84

Table 6: Desolvation energies – version two. Results are in kcal/mol.

Zn^{2+}	CR-1	CR-2	CR-3	CR-4	CR-5*
381.62	39.89	31.49	42.65	46.30	-57.37

Table 7: Electronic binding energies. Results are in kcas/mol.

CR-1	CR-2	CR-3	CR-4	CR-5
-318.75	-661.77	X	X	-599.32

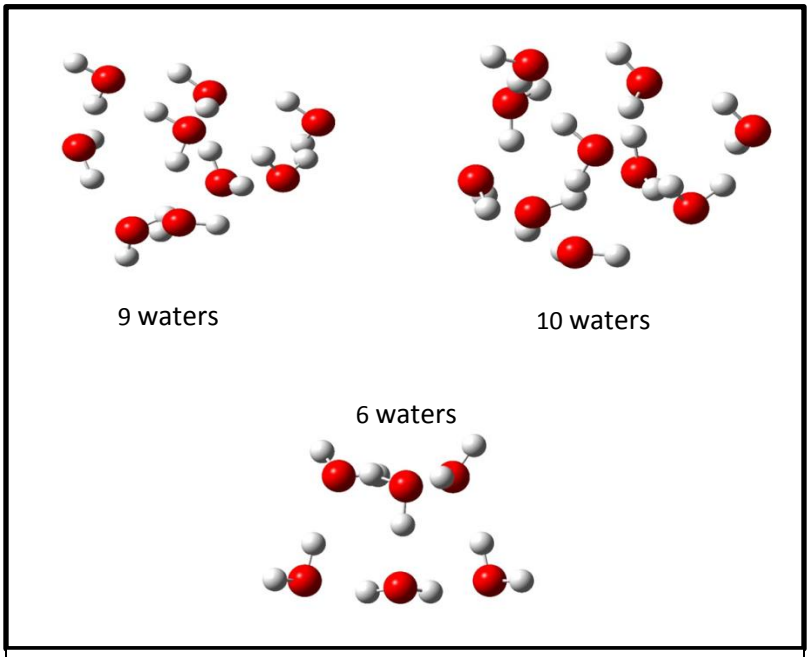

Figure 7: Water cluster structures used in desolvation studies.

Expanded Active Site

Our next step was to study the effect of adding the hydrophobic moiety back onto the molecules. Since CR-2 showed the most promise to be an effective inhibitor of LpxC, we elected to add the hydrophobic moiety to this ligand. CR-2.1 (Figure 13) consists of molecule CR-2 with the addition of one phenyl ring. CR-2.2 (Figure 13) consists of molecule CR-2 with the addition of a biphenyl group. CR-6 (Figure 13) was designed to study the binding of the ligand in the active site without a nucleoside. It has a biphenyl group to serve as its hydrophobic moiety. These optimizations are done with an expanded active site in order to more accurately model the binding of the ligands. This expanded active site includes Lys239, Thr56, His58, His19, Ile18, His265, Gly264, Ala193, Phe161, Glu160, Tyr157, Gly207, Arg262, Gly210, Ser211, Ile201, Ile198, Glu197, Phe194, Phe192, and Gly159. Optimization of CR-2.2 has been completed

(Figure 8), as has optimization of CR-6 (Figure 10). Both CR-6 and CR-2.2 interact with Zn^{2+} via the hydroxamic acid zinc binding motif, as shown in Figures 14 and 15. These optimizations were particularly difficult to obtain since they were optimized in the expanded active site. The larger the active site, the more computational resources are necessary to complete the optimization. This is extremely time intensive.

Most of the interaction energies for CR-2.2 have also been completed, and all of the interaction energies for CR-6 are completed (Table 11). As compared to CR-6, CR-2.2 has the stronger total interaction energy. This could indicate that the uracil portion of our ligands, which CR-6 does not have but CR-2.2 does, could in fact be helpful in the binding of our ligands in the active site. Notably, because CR-6 is a much smaller ligand, the optimization of this ligand took significantly less time than the optimization of CR-2.2. Perhaps, even though CR-2.2 has the stronger interaction energy, for the sake of computational resources, it may make sense to focus more on modeling molecules without the uracil. This could allow us to determine which hydrophobic moiety binds more favorably in the active site while spending less time doing so. I suggest that these ideas should be further investigated in order to arrive at a definitive conclusion. Optimizations of CR-2.1, CR-2.3, L2, L3, and L4 have not yet been completed.

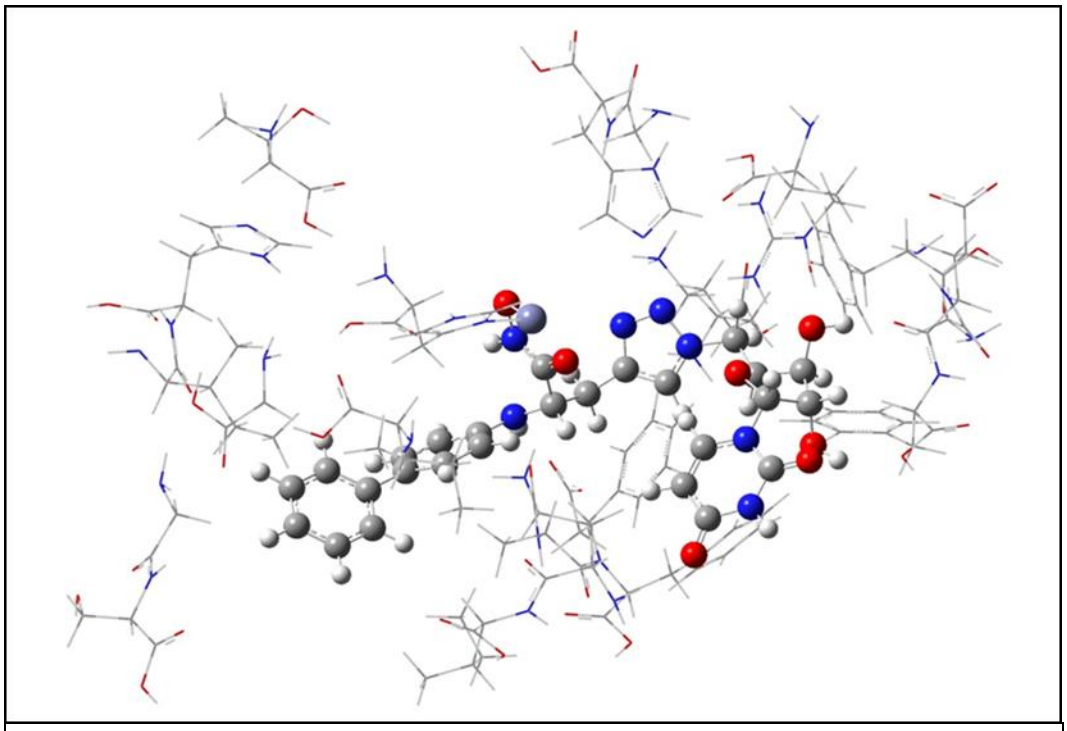

Figure 8: CR-2.2 optimized in the active site of LpxC. The purple atom is Zn^{2+}.

Lys239 and His58 have strong attractive interactions with CR-2.2 (Table 8). This is because the ligand has a -1 charge and both lysine and histidine are positively charged. The glutamate residues in the active site have strong repulsive interactions with CR-2.2 since glutamate is negatively charged, as is our ligand.

Second generation ligands are shown in Figure 9. These are the ligands for which optimizations

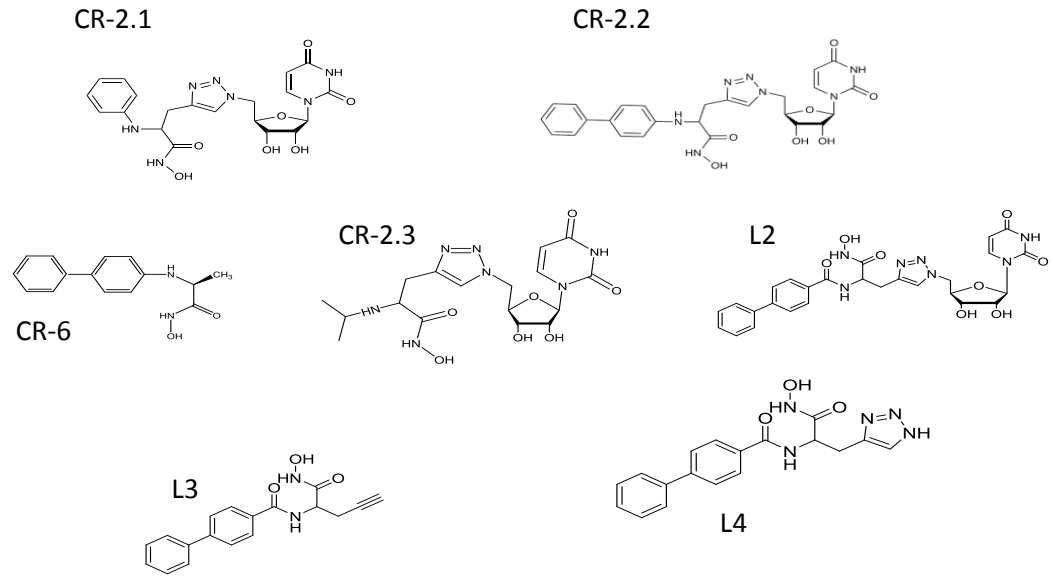

Figure 9: Proposed inhibitors. The linker, nucleoside, and hydrophobic moiety are systematically varied.

have been, or will be done, in an expanded active site.

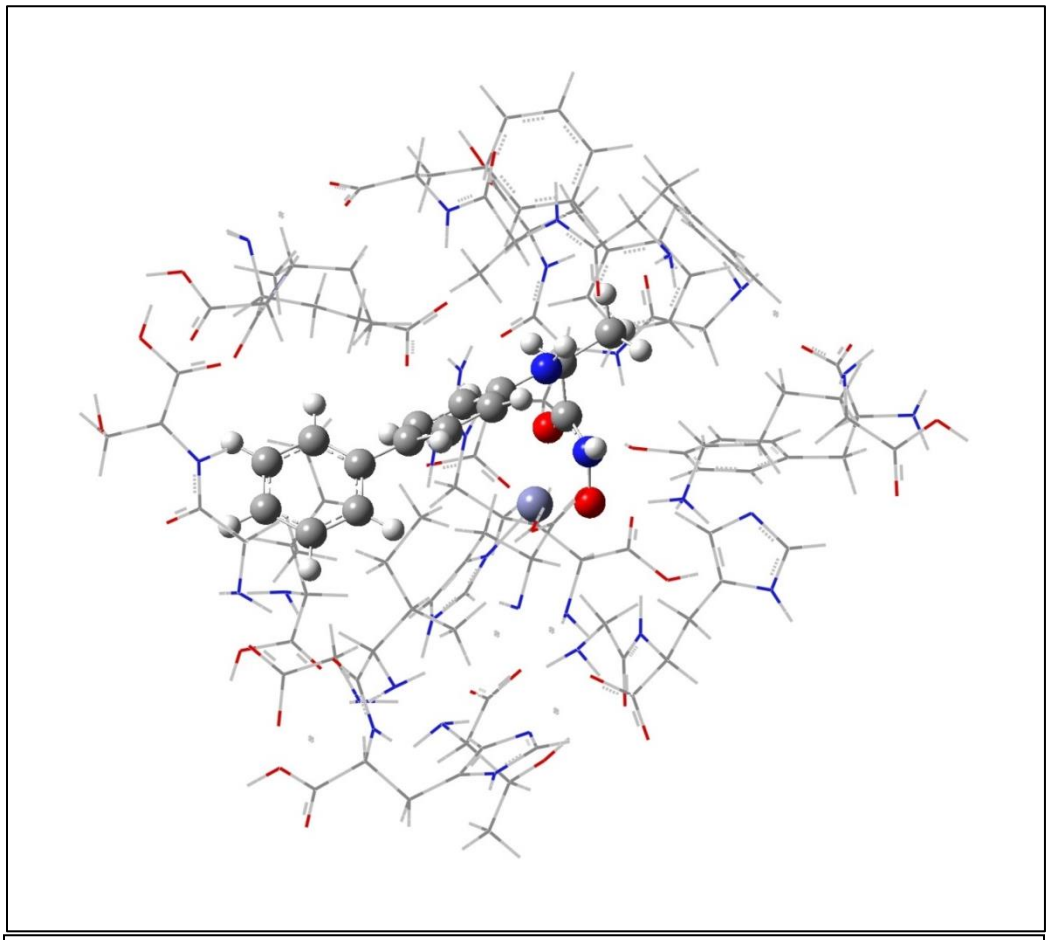

Figure 10: CR-6 optimized complex. The purple atom is Zn^{2+}.

Table 8: Interaction energies for CR-2.2 and CR-6. Results are in kcal/mol.

Residue	CR-2.2	CR-6
Zinc	-470.35	-464.16
Lys	-65.94	-115.89
Thr	0.26	53.61
His 58	-89.61	-0.40
His 19	-2.18	2.17
Ile 18	-1.17	-1.21
His 265	0.82	1.53
Gly 264	-2.97	-7.51
Ala	-6.37	-5.76
Phe 161	-7.09	-4.39
Glu 160	13.05	37.67
Tyr	1.05	-4.93
Gly 207	-4.21	-4.76
Arg	-49.10	-59.05
Gly 210	-2.80	-4.93
Ser	0.72	-1.60
Ile 201	-2.44	-2.81
Ile 198	-1.12	-4.73
Glu 197	38.15	47.30
Phe 194	X	-3.15
Phe 192	X	-1.13
Gly 159	X	-3.10

Total	-651.31	-547.23

Investigation of Zn^{2+} binding

Since Zn^{2+} is the most important in binding our ligands in the LpxC active site, we proposed a set of molecules to study the Zn^{2+} binding more closely. These molecules are shown in Figure 11. Several of the molecules included a carboxyl group rather than a hydroxamic acid. Since we know that the hydroxamic acid is very good at binding Zn^{2+}, we wanted to investigate whether or not a carboxyl group would work as well. If the carboxyl group were to work well, it would indicate to us that we may be able to substitute it for the hydroxamic acid on our proposed inhibitors. The advantage of this would be that these molecules would be significantly simpler to synthesize with a carboxylic acid rather than hydroxamic acid. A collaborator designed a molecule to serve as a model active site. This molecule binds Zn^{2+} such that when the ligands are introduced they can only bind Zn^{2+} once. Our collaborator crystalized his structure with eck serving as the ligand (Figure 12). We were then able to compare the bond lengths of the crystalized structure and the optimized complexes, knowing that if they agree, the crystallization step can be skipped in the future. For the molecules with a carboxyl group, our collaborator's model active site was crystallized with acetate (eckcarboxyl) to serve as a basis for bond length comparisons. Electron excitation energies were also estimated using timedependent DFT. Results are shown in Tables 8 and 9.

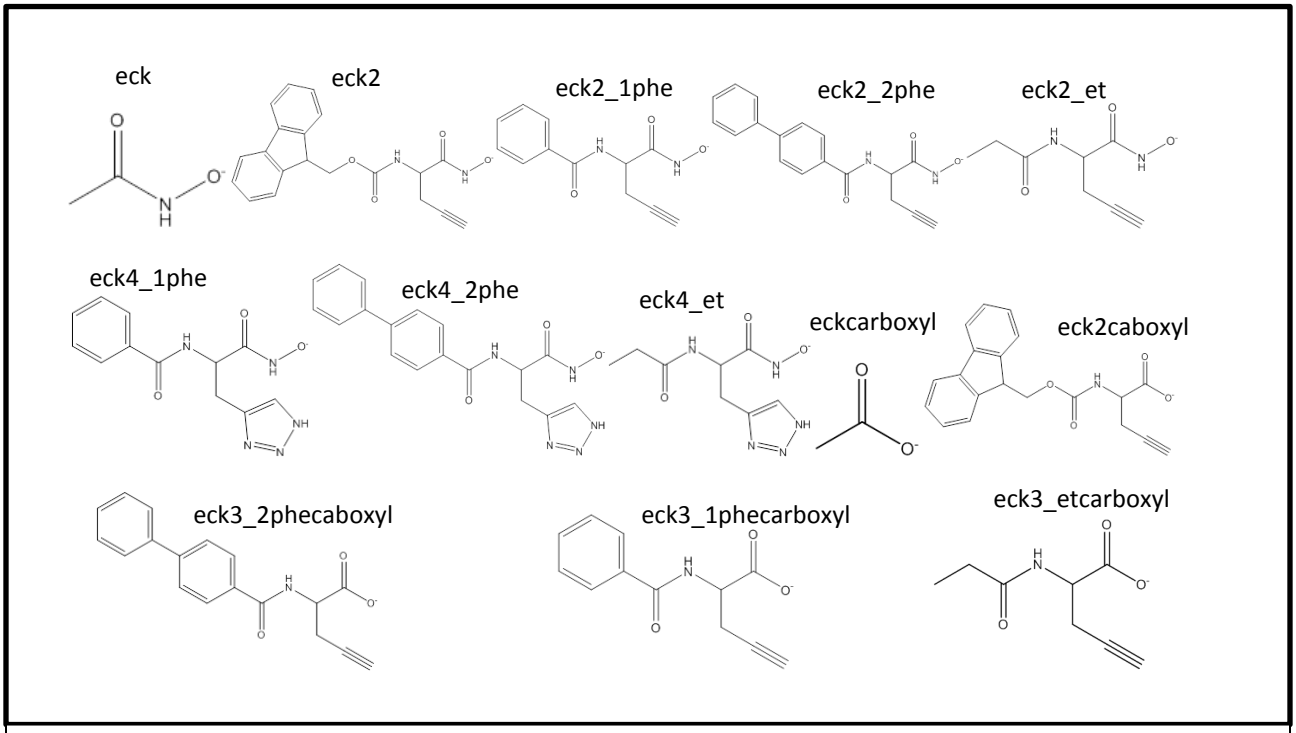

Figure 11: Proposed ligands for Eckenhoff's Zn^{2+} binding model.

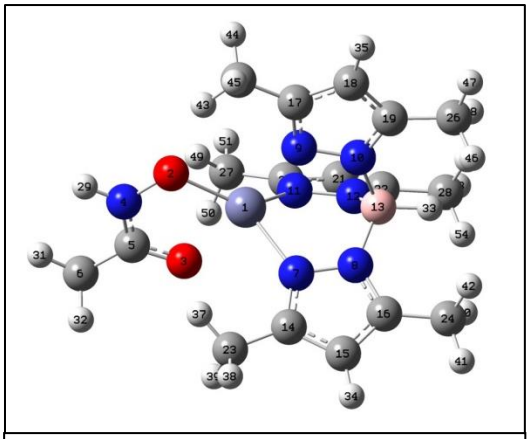

Figure 12: Crystal structure of model active site and eck.

Table 9: Eckenhoff model bond length comparisons and electronic excitation energies. Bond lengths are in angstroms.

		eck	**eck2**	**eck3_1phe**	**eck3_2phe**	**eck3_et**	**eck4_1phe**	**eck4_2phe**	**eck4_et**
	bond length (crystal structure)	bond length (optimized)							
Zn^{2+} and nitrogen 1 (7)	2.04037	2.04295	2.04788	2.04436	2.04973	2.04667	2.05572	2.05402	2.05109
Zn^{2+} and nitrogen 2 (9)	2.17592	2.15491	2.13372	2.13805	2.1315	2.12875	2.10854	2.1164	2.11853
Zn^{2+} and nitrogen 3 (11)	2.03753	2.04634	2.04811	2.04945	2.04393	2.04483	2.04406	2.04761	2.04895
Zn^{2+} and oxygen 1 (2)	1.95367	2.01409	2.02085	2.00697	2.00986	2.00849	2.0133	2.01158	2.01581
Zn^{2+} and oxygen 2 (3)	2.19209	2.16073	2.17457	2.19274	2.17637	2.18191	2.17644	2.18926	2.16202
Excited State 1		313.02 nm	382.8 nm	7152.05 nm	6400.70 nm	3362.52 nm	428.32 nm	368.47 nm	465.78 nm
Excited State 2		307.77 nm	329.62 nm	1489.54 nm	1468.79 nm	1321.83 nm	334.77 nm	310.45 nm	359.74 nm
Excited State 3		258.79 nm	307.52 nm	1177.24 nm	1156.10 nm	1006.94 nm	333.29 nm	304.82 nm	343.65 nm

Eck3_1phe, eck3_2phe, and eck3_et had abnormally large excited states (Table 9). It is unlikely that these results are accurate. We are going to try another method of approximating these numbers in an attempt to get a more accurate result.

The molecular orbitals for the eckenhoff model excited states can be seen in Figures 13 and 14.

Table 10: Carboxyl Eckenhoff model bond length comparisons and electronic excitation energies. Bond lengths are in angstroms.

		eckcarboxyl (w/o solvent)	**eck2 carboxyl**	**eck3_1phe carboxyl**	**eck3_2phe carboxyl**	**eck3_et carboxyl**
	bond length (acetate crystal structure)	bond length (optimized)				
Zn^{2+} and nitrogen 1 (5)	2.01574	2.01791	2.03633	2.03258	2.03347	2.02397
Zn^{2+} and nitrogen 2 (7)	2.05145	2.06792	2.06128	2.04956	2.05938	2.06461
Zn^{2+} and nitrogen 3 (9)	2.00956	2.01791	2.02411	2.01908	2.02104	2.02954
Zn^{2+} and oxygen 1 (2)	2.60349	2.34965	2.36822	2.47425	2.38322	2.38031
Zn^{2+} and oxygen 2 (86)	1.92228	2.03234	2.04931	2.01098	2.03817	2.03362
Excited State 1		260.05 nm	289.28 nm	317.04 nm	339.49 nm	247.04 nm
Excited State 2		254.25 nm	280.8 nm	308.06 nm	326.55 nm	244.84 nm
Excited State 3		247.07 nm	278.17 nm	303.59 nm	323.51 nm	244.12 nm

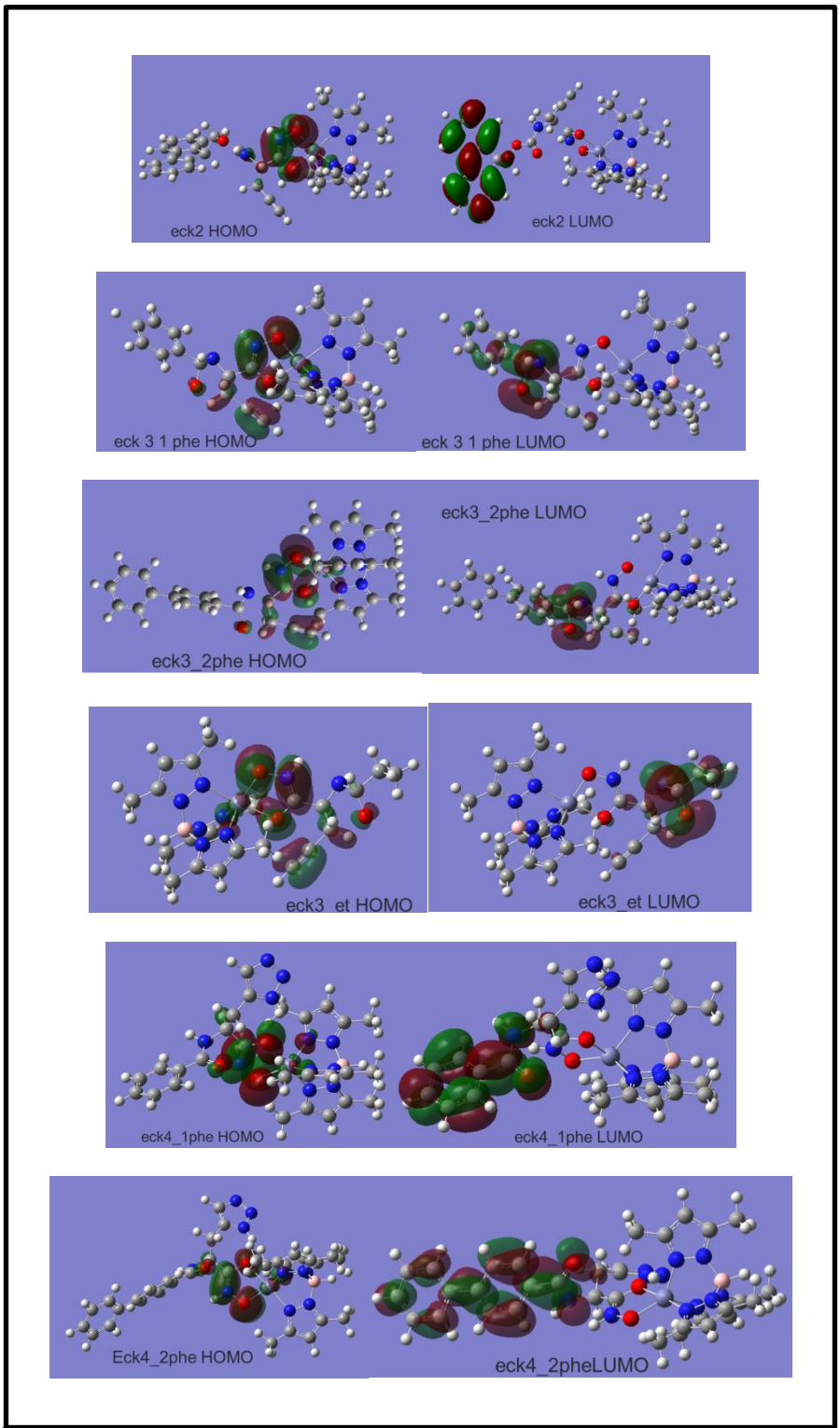

Figure 13: Molecular orbitals for the hydroxamic acid eckenhoff model excited states

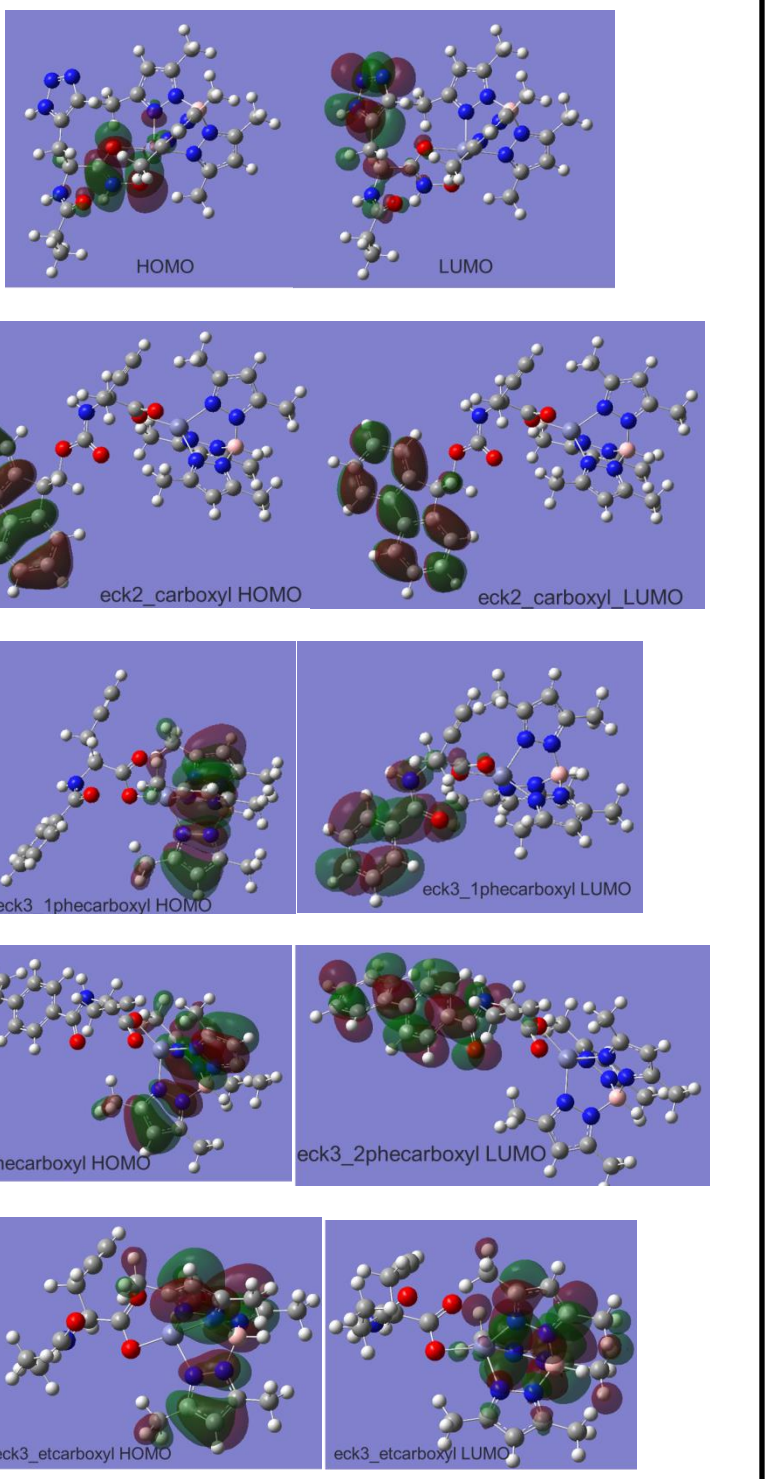

Figure 14: Molecular orbitals for the carboxyl eckenhoff model excited states

Log P and Log D Calculations

Log P and Log D were calculated for the eckenhoff ligands, as well as for CR-6, CR-2, L2, L3, and L4. These values tell us about the pharmacokinetics, which gives us information about transport in blood, cytosol, and the cell membrane, including ease of absorption. LogP was determined for ligands with all ionizable substituents fully protonated, while LogD considers the ligand at physiological pH. All of the values for Log D and Log P were below 5. This indicates that these molecules should be orally active, as they follow Lipinski's Rule of Five.[24] However, the fact that the values are so negative could suggest that these molecules will encounter issues crossing membranes. Log P values for the protonated forms of the molecules are shown in Table 11. Log P values for the deprotonated forms of the molecules are shown in Table 12. Log D values are shown in Table 13.

Table 11: Log P for the protonated forms of the molecules

Molecule	Log P
CR-6	-1.67913
Eck	-1.08921
Eck2	-2.37944
Eck3_1phe	-2.67922
Eck3_2phe	-2.48274
Eck3_et	-2.08068
Eck4_1phe	-3.08229
Eck4_2phe	-2.48224
Eck4_et	-2.99874
Eckcarboxyl	-0.5641
Eck2_carboxyl	-1.80117
Eck3_1phecarboxyl	-1.80471
Eck3_2phecarboxyl	-1.58495
Eck3_etcarboxyl	-1.83307
CR-2	-2.91
L2	0.55
L3	-1.05
L4	-7.78

Table 12: Log P for the deprotonated forms of the molecules

Molecule	Log P
CR-6	-6.45169
Eck	-5.78733
Eck2	-7.32518
Eck3_1phe	-7.18542
Eck3_2phe	-6.4365
Eck3_et	-7.3586
Eck4_1phe	-6.71906
Eck4_2phe	-6.91249
Eck4_et	-7.06136
Eckcarboxyl	-5.1098
Eck2_carboxyl	-6.21015
Eck3_1phecarboxyl	-6.9925
Eck3_2phecarboxyl	-6.94439
Eck3_etcarboxyl	-6.13723
CR-2	-9.53
L2	X
L3	-6.40
L4	-1.51

Table 13: Log D values

Molecule	Log D
CR-6	-1.67913
Eck	-1.08921
Eck2	-2.37944
Eck3_1phe	-2.67922
Eck3_2phe	-2.48274
Eck3_et	-2.08068
Eck4_1phe	-3.08229
Eck4_2phe	-2.48224
Eck4_et	-2.99874
Eckcarboxyl	-0.5641
Eck2_carboxyl	-1.80117
Eck3_1phecarboxyl	-1.80471
Eck3_2phecarboxyl	-1.58495
Eck3_etcarboxyl	-1.83307
CR-2	X
L2	X
L3	X
L4	X

4. Conclusions

From our initial work with a truncated active site, CR-2 showed considerable promise as an inhibitor of LpxC.

Studying the zinc binding models showed that the hydroxamic acid bound zinc much better than did the carboxylic acid.

While further research is definitely required to narrow down the list of potential antibacterial agents, it can be concluded from my research with the expanded active site that CR-2.2 shows considerable promise. Additionally, due to the extreme amount of time and computational resources required to optimize ligands in the expanded active site, I would suggest that all further optimizations be done in the truncated active site. While the expanded active site is a more realistic model, the truncated active site only seems to be slightly less realistic and takes a considerably shorter amount of time and less computational resources to complete optimizations in.

Further research should be done to compare hydrophobic moieties, or more generally, to determine whether or not a hydrophobic moiety is necessary. Optimization and calculation of interaction energies for CR-2 in the expanded active site would allow us to directly compare a molecule with and without the hydrophobic moiety. Furthermore, it is possible that a phenyl ring could be better than the biphenyl, or that an acyclic hydrocarbon may confer some advantage. This should be studied.

The question of whether or not the uracil and linker portions are completely necessary also warrants further research.

Additionally, research should be done in order to determine whether the negative LogD and LogP results are in fact good results, given that even though they follow Lipinski's Rule of Five, they are quite negative.

5. References

[1] Vaara, M., Lipid A: target for antibacterial drugs. Science 1996, 274, (5289), 939-940.

[2] Li, X.; McClerren, A. L.; Raetz, C. R. H.; Hindsgaul, O., Mapping the active site of the bacterial enzyme LpxC using novel carbohydrate-based hydroxamic acid inhibitors. J. Carbohydr. Chem. 2005, 24, (4-6), 583-609.

[3] Murphy, S. L.; Xu, J.; Kochanek, K. D., Deaths: Preliminary Data for 2010. Natl. Vital Stat. Rep. 2012, 60, (4), 1-50.

[4] Jackman, J. E.; Fierke, C. A.; Tumey, L. N.; Pirrung, M.; Uchiyama, T.; Tahir, S. H.; Hindsgaul, O.; Raetz, C. R. H., Antibacterial agents that target lipid A biosynthesis in gram-negative bacteria: inhibition of diverse UDP-3-O-(R-3-hydroxymyristoyl)-N-acetylglucosamine deacetylases by substrate analogs containing zinc binding motifs. J. Biol. Chem. 2000, 275, (15), 11002-11009.

[5] Onishi, H. R.; Pelak, B. A.; Gerckens, L. S.; Silver, L. L.; Kahan, F. M.; Chen, M.-H.; Patchett, A. A.; Galloway, S. M.; Hyland, S. A.; et al., Antibacterial agents that inhibit lipid A biosynthesis. Science (Washington, D. C.) 1996, 274, (5289), 980-982.

[6] Pirrung, M. C.; Tumey, L. N.; McClerren, A. L.; Raetz, C. R. H., High-Throughput Catch-and-Release Synthesis of Oxazoline Hydroxamates. Structure-Activity Relationships in Novel Inhibitors of Escherichia coli LpxC: In Vitro Enzyme Inhibition and Antibacterial Properties. J. Am. Chem. Soc. 2003, 125, (6), 1575-1586.

[7] Coggins, B. E.; McClerren, A. L.; Jiang, L.; Li, X.; Rudolph, J.; Hindsgaul, O.; Raetz, C. R. H.; Zhou, P., Refined Solution Structure of the LpxC-TU-514 Complex and pKa Analysis of an Active Site Histidine: Insights into the Mechanism and Inhibitor Design. Biochemistry 2005, 44, (4), 1114-1126.

[8] McClerren, A. L.; Endsley, S.; Bowman, J. L.; Andersen, N. H.; Guan, Z.; Rudolph, J.; Raetz, C. R. H., A Slow, Tight-Binding Inhibitor of the Zinc-Dependent Deacetylase LpxC of Lipid A Biosynthesis with Antibiotic Activity Comparable to Ciprofloxacin. Biochemistry 2005, 44, (50), 16574-16583.

[9] Kline, T.; Andersen, N. H.; Harwood, E. A.; Bowman, J.; Malanda, A.; Endsley, S.; Erwin, A. L.; Doyle, M.; Fong, S.; Harris, A. L.; Mendelsohn, B.; Mdluli, K.; Raetz, C. R. H.; Stover, C. K.; Witte, P. R.; Yabannavar, A.; Zhu, S., Potent, Novel in Vitro Inhibitors of the Pseudomonas aeruginosa Deacetylase LpxC. J. Med. Chem.2002, 45, (14), 3112-3129.

[10] Clements, J. M.; Coignard, F.; Johnson, I.; Chandler, S.; Palan, S.; Waller, A.; Wijkmans, J.; Hunter, M. G., Antibacterial activities and characterization of novel inhibitors of LpxC. Antimicrob. Agents Chemother. 2002, 46, (6), 1793-1799.

[11] McAllister, L. A.; Montgomery, J. I.; Abramite, J. A.; Reilly, U.; Brown, M. F.; Chen, J. M.; Barham, R. A.; Che, Y.; Chung, S. W.; Menard, C. A.; Mitton-Fry, M.; Mullins, L. M.; Noe, M. C.; O'Donnell, J. P.; Oliver, R. M.; Penzien, J. B.; Plummer, M.; Price, L. M.; Shanmugasundaram, V.; Tomaras, A. P.; Uccello, D. P., Heterocyclic methylsulfone hydroxamic acid LpxC inhibitors as Gram-negative antibacterial agents. Bioorg. Med. Chem. Lett. 2012, 22, (22), 6832-6838.

[12] Brown, M. F.; Reilly, U.; Abramite, J. A.; Arcari, J. T.; Oliver, R.; Barham, R. A.; Che, Y.; Chen, J. M.; Collantes, E. M.; Chung, S. W.; Desbonnet, C.; Doty, J.; Doroski, M.; Engtrakul, J. J.; Harris, T. M.; Huband, M.; Knafels, J. D.; Leach, K. L.; Liu, S.; Marfat, A.; Marra, A.; McElroy, E.; Melnick, M.; Menard, C. A.; Montgomery, J. I.; Mullins, L.; Noe, M. C.; O'Donnell, J.; Penzien, J.; Plummer, M. S.; Price, L. M.; Shanmugasundaram, V.; Thoma, C.; Uccello, D. P.; Warmus, J. S.; Wishka, D. G., Potent Inhibitors of LpxC for the Treatment of Gram-Negative Infections. J. Med. Chem. 2011, 55, (2), 914-923.

[13] Barb, A. W.; Leavy, T. M.; Robins, L. I.; Guan, Z. Q.; Six, D. A.; Zhou, P.; Bertozzi, C. R.; Raetz, C. R. H., Uridine-Based Inhibitors as New Leads for Antibiotics Targeting Escherichia coli LpxC. Biochemistry 2009, 48, (14), 3068-3077.

[14] Barb, A. W.; Jiang, L.; Raetz, C. R. H.; Zhou, P., Structure of the deacetylase LpxC bound to the antibiotic CHIR-090: Time-dependent inhibition and specificity in ligand binding. Proc. Natl. Acad. Sci. U. S. A. 2007, 104, (47), 18433-18438.

[15] Barb, A. W.; Zhou, P.Mechanism and inhibition of LpxC: an essential zinc-dependent deacetylase of bacterial lipid A synthesis. Curr. Pharm. Biotechnol. 2008, 9, 9-15;

[16] Gaussian 09, Revision C.01, M. J. Frisch, G. W. Trucks, H. B. Schlegel, G. E. Scuseria, M. A. Robb, J. R. Cheeseman, G. Scalmani, V. Barone, B. Mennucci, G. A. Petersson, H. Nakatsuji, M. Caricato, X. Li, H. P. Hratchian, A. F. Izmaylov, J. Bloino, G. Zheng, J. L. Sonnenberg, M. Hada, M. Ehara, K. Toyota, R. Fukuda, J. Hasegawa, M. Ishida, T. Nakajima, Y. Honda, O. Kitao, H. Nakai, T. Vreven, J. A. Montgomery, Jr., J. E. Peralta, F. Ogliaro, M. Bearpark, J. J. Heyd, E. Brothers, K. N. Kudin, V. N. Staroverov, R. Kobayashi, J. Normand, K. Raghavachari, A. Rendell, J. C. Burant, S. S. Iyengar, J. Tomasi, M. Cossi, N. Rega, J. M. Millam, M. Klene, J. E. Knox, J. B. Cross, V. Bakken, C. Adamo, J. Jaramillo, R. Gomperts, R. E. Stratmann, O. Yazyev, A. J. Austin, R. Cammi, C. Pomelli, J. W. Ochterski, R. L. Martin, K. Morokuma, V. G. Zakrzewski, G. A. Voth, P. Salvador, J. J. Dannenberg, S. Dapprich, A. D. Daniels, Ö. Farkas, J. B. Foresman, J. V. Ortiz, J. Cioslowski, and D. J. Fox, Gaussian, Inc., Wallingford CT, 2009.

[17] Wang, Y: Babin, V; Bowman, J.M; Paesani, F; The water hexamer: cage, prism, or both. Full dimensional quantum simulations say both. J. Am. Chem. Soc. 134 (2012) 11116-11119; 8.

[18] Perez, C; Zaleski D.P; Seifert, N.A; Temelso, B; Shields G.C; Kisiel, Z; Pate, B.H; Hydrogen bond cooperativity and the three-dimensional structures of water nonamers and decamers. Angew. Chem. Int. Ed. 53 (2014) 14368-14372.

[19] Hatstat, A.K; Morris, M. Peterson, L.W; Cafiero, M; Ab initio study of electronic interaction energies and desolvation energies for dopaminergic ligands in the catechol-O-methyltransferase active site. Computational and Theoretical Chemistry. 1078 (2016) 146–162

[20]Zhang, S; Baker J; Peter Pulay; A reliable and efficient first principles-based method for predicting pKa Values. 1. Methodology. J. Phys. Chem. 114 (2010) 425-431

[21]Zhang, S; Baker J; Peter Pulay; A reliable and efficient first principles-based method for predicting pKa Values. 2. Organic Acids. J. Phys. Chem. 114 (2010) 432-4442

[22]Zhao, Y; D.G. Truhlar; A new local density functional for main-group thermochemistry, transition metal bonding, thermochemical kinetics, and noncovalent interactions. (2006) J. Chem. Phys.. 125 (19): 194101.

[23]Mennucci, B; Polarizable continuum model. Wiley Interdisciplinary Reviews: Computational Molecular Science. 2 (2012) 386-404.

[24]Lipinski, C.A; Lombardo, F; Dominy, B.W.; Feeney, P.J.; Experimental and computational approaches to estimate solubility and permeability in drug discovery and development settings. Adv. Drug Deliv. Rev. 2012, 64: 4-17.